

Supporting information

Design and Fabrication of Phosphazene-based Porous Organic Materials for Iodine Adsorption

*Yichao, Wu,*¹ *Qianyi, Zuo,*^{1,2} *Tao, Jiang,*¹ *Zilong Wang,*¹ *Jia Hong Pan,*² *Zhuoyu, Ji*^{1,*}

¹ MOE Key Laboratory of Resources and Environmental Systems Optimization, College of Environmental Science and Engineering, North China Electric Power University, Beijing 102206, China

² State Key Laboratory of Featured Metal Materials and Life-Cycle Safety for Composite Structures, School of Resources, Environments and Materials, Guangxi University, Nanning 530004, China

* Corresponding author: Zhuoyu, Ji (jizhuoyu@ncepu.edu.cn)

Table of contents

1. Materials characterization:	1
2. Additional synthetic and experimental methods	2
Scheme S1 Synthesis route of X-HCCP.	9
Scheme S2 Synthesis route of TAPA-HCCP and TAPDA-HCCP.	11
Fig. S1 FT-IR spectroscopy.	12
Fig. S2 XRD patterns.	13
Fig. S3 XPS spectra of N1s.	14
Fig. S4 SEM images.	15
Fig. S5 TGA curve.	16
Fig. S6 N₂ adsorption-desorption isotherms and pore size distribution	17
Fig. S7 Color change of materials.	18
Fig. S8 Summary of the I₂ vapor adsorption performance.	19
Fig. S9 Kinetic model diagram of iodine vapor adsorption.	20
Fig. S10 The color change of iodine solution.	21
Fig. S11 Water contact angle diagram.	22
Fig. S12 The first-order kinetic model of iodine solution and the Freundlich model.	23
Fig. S13 Comparison chart of iodine water properties.	24
Fig. S14 Kinetic model of iodine ion adsorption.	25
Fig. S15 The first-order kinetic model and Freundlich model of methyl iodide and iodocyclohexane.	26
Fig. S16 Adsorption penetration curve.	27
Fig. S17 Iodine vapor and iodine water reusability experiment.	28
Fig. S18 Methyl iodide reusability experiment.	29
Fig. S19 FT-IR spectra before and after iodine vapor adsorption.	30
Fig. S20 XPS spectrum of BDD-HCCP.	31
Fig. S21 XPS spectra of P 2p.	32
Table of experimental dates and other information.	33
References	46

1. Materials characterization:

The surface morphology of the materials was observed using a TESCAN MIRA LMS scanning electron microscope (SEM). Fourier transform infrared (FT-IR) spectra were recorded using a SHIMADZU-IRT Racer-100 spectrometer with potassium bromide (KBr) as the background and solid dispersant. The crystalline structure was analyzed by X-ray diffraction (XRD) on a Rigaku Smart Lab diffractometer in the 2θ range of 5 to 40° using Cu $K\alpha$ radiation. X-ray photoelectron spectroscopy (XPS) measurements were performed on a Thermo Fisher Nexsa instrument. Thermogravimetric analysis (TGA) was conducted on a HITACHI STA200 instrument under a nitrogen atmosphere, with a temperature range of 25 to 800°C and a heating rate of $10^\circ\text{C}\cdot\text{min}^{-1}$. Water contact angle (WCA) measurements were made using a Kruss DSA25 contact angle goniometer. Absorption spectra were recorded with a Shimadzu UV-2700 UV-Vis spectrophotometer.

2. Additional synthetic and experimental methods

2.1 Synthesis of BDP-HCCP :

To synthesize BDP-HCCP, BDP (0.552 g, 3 mmol) and HCCP (0.347 g, 1 mmol) were added to a pressure-resistant, thick-walled vial containing 1.5 mL of triethylamine in 20 mL 1,4-dioxane. The solution was sonicated for 30 min to ensure uniform dispersion of the solute, followed by nitrogen purging for 10 min. The resulting mixture was heated at 100°C in an oil bath for 72 h with continuous stirring at 500 rpm. After filtering the solvent, the solid product was washed sequentially with water, 1,4-dioxane, THF and ethanol. The final product was vacuum-dried overnight at 60°C , yielding a green powder.

2.2 Synthesis of BDD-HCCP

To synthesize BDD-HCCP, and HCCP (0.347 g, 1 mmol) were added to a pressure-resistant, thick-walled vial containing 1.5 mL of triethylamine in 20 mL 1,4-dioxane. The solution was sonicated

for 20 min to ensure uniform dispersion of the solute, followed by nitrogen purging for 10 min. The resulting mixture was heated at 100°C in an oil bath for 72 h with continuous stirring at 500 rpm. After filtering the solvent, the solid product was washed sequentially with water, 1,4-dioxane, THF and ethanol. The final product was vacuum-dried overnight at 60°C, yielding a yellow powder.

2.3 Synthesis of TAPA-HCCP

To synthesize TAPA-HCCP, TAPA (0.174 g, 0.6 mmol), and HCCP (0.208 g, 0.6 mmol) were added to a pressure-resistant, thick-walled vial containing 1.35 mL of triethylamine in N,N-Dimethylformamide (DMF). The solution was sonicated for 20 min to achieve uniform solute dispersion, followed by nitrogen purging for 10 min. The resulting mixture was then heated at 100°C in an oil bath for 72 h with continuous stirring at 500 rpm. After filtering the solvent, the obtained solid was washed sequentially with water, dioxane, and ethanol. Finally, the product was vacuum-dried overnight at 60°C, yielding a yellow powder.

2.4 Gas-phase iodine adsorption experiment

Iodine Vapor: In this experiment, the adsorption capacity of iodide vapor was primarily tested using a gravimetric method. First, 10 mg of adsorbent and a specific amount of iodine pellets were placed in a small weighing vial. The vial was then placed in a sealed container and heated in an oven at 348.15 K for adsorption. At different time intervals (0.5, 1, 2, 4, 8, 12, 24, 48, 72, 96, 120, and 180 h), the vial containing the adsorbent and an empty reference vial were weighed to eliminate interference. Finally, the adsorption capacity was calculated using the appropriate formula (Eq. (1)):

$$q_e = \frac{g_t - g_0 - g_b}{g_0} \quad (1)$$

Here, q_e represents the adsorption capacity per gram of adsorbent at a given time (min), g_t and g_0

are the post-adsorption and initial weights of the vial containing the adsorbent (g), respectively, and g_b is the weight of the blank reference vial (g).

Methyl iodide: The adsorption capacity of methyl iodide vapor was measured using a gravimetric method. A specified amount of methyl iodide solution was placed in a pressure-resistant vial, and 10 mg of adsorbent was weighed into a small weighing vial, which was then placed inside the sealed pressure-resistant vial. The setup was placed in an oven at 348.15 K for adsorption. At different time intervals (0, 12, 4, 8, 12, 24, 48, 72 h), the weighing vial containing the adsorbent, as well as an empty reference vial, were weighed to eliminate interference. The adsorption capacity was calculated using the following formula (Eq. (2)):

$$q_e = \frac{g_t - g_0 - g_b}{g_0} \quad (2)$$

Here, q_e represents the adsorption capacity per gram of adsorbent at a given time (min), g_t and g_0 are the post-adsorption and initial weights of the vial containing the adsorbent (g), respectively, and g_b is the weight of the blank reference vial (g).

We used the pseudo-first-order reaction model and the pseudo-second-order kinetic equation to fit the kinetic data of the iodine vapor adsorption experiment. The calculation formulas are as follows (Eqs. (3) and (4)):

Pseudo-first-order reaction model:

$$q_t = q_e(1 - e^{-k_1 t}) \quad (3)$$

Pseudo-second-order kinetic equation:

$$\frac{t}{q_t} = \frac{1}{k_2 q_e^2} + \frac{t}{q_e} \quad (4)$$

where t is the adsorption time (h), q_t is the adsorption capacity at time t ($\text{g}\cdot\text{g}^{-1}$), q_e is the

equilibrium adsorption capacity, k_1 is the pseudo-first-order rate constant (h^{-1}), and k_2 is the pseudo-second-order rate constant ($\text{g}\cdot\text{g}^{-1}\cdot\text{h}^{-1}$).

2.5 Detailed procedure for capturing liquid-phase iodine

Iodine Solution: To study the adsorption kinetics of the adsorbent in iodine aqueous solution, the adsorbent was added to a $100 \text{ mg}\cdot\text{L}^{-1}$ iodine solution at a solid-to-liquid ratio of $0.1 \text{ g}\cdot\text{L}^{-1}$. Samples were taken at different time intervals (0, 10, 25, 60, 120, 240, 360, 720, 1440 min), and the residual iodine concentration in the solution was measured using a UV-Vis spectrophotometer at a wavelength of 461 nm. The removal efficiency E (%) of the adsorbent was calculated using the following formula (Eq. (5)):

$$E = \frac{C_0 - C_t}{C_0} \times 100\% \quad (5)$$

Where C_0 is the initial iodine concentration ($\text{mg}\cdot\text{L}^{-1}$), and C_t is the iodine concentration at time t ($\text{mg}\cdot\text{L}^{-1}$).

Iodine in Cyclohexane: To study the adsorption kinetics of the adsorbent in iodine cyclohexane solution, the adsorbent was added to a $200 \text{ mg}\cdot\text{L}^{-1}$ iodine cyclohexane solution at a solid-to-liquid ratio of $1 \text{ g}\cdot\text{L}^{-1}$. Samples were taken at different time intervals (0, 5, 15, 30, 60, 120, 240, 480, 720, and 1440 min), and the residual iodine concentration in the solution was measured using a UV-Vis spectrophotometer at a wavelength of 523 nm. The removal efficiency E (%) of the adsorbent was calculated using the following formula (Eq. (6)):

$$E = \frac{C_0 - C_t}{C_0} \times 100\% \quad (6)$$

Where C_0 is the initial iodine concentration ($\text{mg}\cdot\text{L}^{-1}$), and C_t is the iodine concentration at time t ($\text{mg}\cdot\text{L}^{-1}$).

Iodine Ion Solution: To study the adsorption kinetics of the adsorbent in iodine ion solution, the adsorbent was added to a 50 mg L⁻¹ iodine ion solution at a solid-to-liquid ratio of 0.1 g L⁻¹. Samples were taken at different time intervals (0, 5, 15, 30, 60, 120, 240, and 360 min), and the residual iodine concentration in the solution was measured using a UV-Vis spectrophotometer at a wavelength of 288 nm. The removal efficiency E(%) of the adsorbent was calculated using the following formula (Eq. (7)):

$$E = \frac{C_0 - C_t}{C_0} \times 100 \quad (7)$$

Where C₀ is the initial iodine concentration (mg L⁻¹), and C_t is the iodine concentration at time t (mg L⁻¹).

The pseudo-first-order reaction model and the pseudo-second-order kinetic equation were used by us to fit the kinetic model of iodine vapor adsorption experiments. The calculation formulas are as follows (Eqs. (8) and (9)):

Pseudo-first-order reaction model:

$$q_t = q_e(1 - e^{-k_1 t}) \quad (8)$$

Pseudo-second-order kinetic model:

$$\frac{t}{q_t} = \frac{1}{k_2 q_e^2} + \frac{t}{q_e} \quad (9)$$

In the equations, t is the adsorption time (min), q_t is the adsorption amount at time t (g·g⁻¹), q_e is the equilibrium adsorption capacity (g·g⁻¹), k₁ is the pseudo-first-order rate constant (min⁻¹), and k₂ is the pseudo-second-order rate constant (g·g⁻¹·min⁻¹).

2.6 Liquid-phase isotherm experiment

Iodine Solution: A stock solution of iodine water at 200 mg L⁻¹ was prepared and subsequently diluted to concentrations of 10, 20, 40, 60, 80, 100, 120 and 160 mg L⁻¹.

The adsorption capacity and removal efficiency were calculated according to the following (Eq. (10)):

$$q_e = \frac{(C_0 - C_e) \times V}{m} \quad (10)$$

In the equation, C₀ is the initial concentration of iodine in the solution (mg L⁻¹), C_e is the equilibrium concentration of iodine (mg L⁻¹), V is the volume of the solution added (L), and m is the mass of the adsorbent added (g).

Iodine Cyclohexane: In this experiment, a stock solution of iodine cyclohexane at 5000 mg L⁻¹ was prepared and then diluted to various concentrations: 200, 250, 300, 400, 500, 600, 800, and 1000 mg·L⁻¹. The equilibrium adsorption capacity of the adsorbent for each iodine cyclohexane concentration is then calculated using the above equation. The adsorption capacity and removal efficiency were calculated according to the following (Eq. (11)):

$$q_e = \frac{(C_0 - C_e) \times V}{m} \quad (11)$$

In the equation, C₀ is the initial concentration of iodine in the solution (mg·L⁻¹), C_e is the equilibrium concentration of iodine (mg L⁻¹), V is the volume of the solution added (L), and m is the mass of the adsorbent added (g).

The adsorption isotherms were fitted using the typical Langmuir and Freundlich models to determine the type of adsorption behavior for the materials. The Langmuir and Freundlich adsorption models are expressed as follows (Eqs. (12) and (13)):

Langmuir isotherm:

$$q_e = \frac{C_e q_m K_L}{1 + K_L C_e} \quad (12)$$

Where Q_e is the equilibrium adsorption capacity ($\text{mg}\cdot\text{g}^{-1}$), C_e is the equilibrium concentration of iodine (mg L^{-1}), q_m is the maximum adsorption capacity ($\text{mg}\cdot\text{g}^{-1}$), K_L is the Langmuir equilibrium adsorption constant ($\text{L}\cdot\text{mg}^{-1}$).

Freundlich isotherm:

$$q_e = K_F C_e^{\frac{1}{n}} \quad (13)$$

Where q_e is the equilibrium adsorption capacity ($\text{mg}\cdot\text{g}^{-1}$), C_e is the equilibrium concentration of iodine (mg L^{-1}), K_F is the Freundlich constant ($\text{mg}^{1-n}\cdot\text{L}^n\cdot\text{g}^{-1}$), $1/n$ is the adsorption intensity, where n is a measure of the adsorption strength.

By applying these models to the experimental data, you can determine the adsorption type and characteristics of the material based on the values of the constants q_m , K_L , K_F , and $1/n$.

2.7 Iodine Water Breakthrough Experiment

The iodine water breakthrough experiment was conducted to investigate the dynamic adsorption capacity of the adsorbent for iodine in water. The experiment was carried out using a peristaltic pump, and the tubing used in the experiment was saturated tubing. The experimental setup is shown in the diagram below.

The maximum dynamic adsorption capacity Q_e ($\text{mg}\cdot\text{g}^{-1}$) of the adsorbent in the iodine water solution is calculated from the breakthrough curve using the following equation (Eq. (14)):

$$Q_e = \frac{\int_0^{V_2} (C_0 - C_{V_2}) dV_2 - \int_0^{V_1} (C_0 - C_{V_1}) dV_1}{m} \quad (14)$$

Where, m is the mass of the adsorbent (g), C_0 is the initial iodine concentration (mg L^{-1}), C_{v1} is the iodine concentration in the effluent when no adsorbent is packed (mg L^{-1}), C_{v2} is the iodine concentration in the effluent when the adsorbent is packed ($\text{mg}\cdot\text{L}^{-1}$).

2.8 Material Recyclability Experiment

This experiment uses ethanol immersion to recover iodine adsorbed by the material and conducts adsorption cycle experiments on the material.

Iodine Vapor Cycling: 20 mg of adsorbent is added to a 10 mL vial containing elemental iodine (≥ 1 g). The mixture is then adsorbed at 348.15 K for 72 h until adsorption equilibrium is reached. Afterward, the iodine adsorption capacity of the adsorbent is measured by the weighing method. The adsorption capacity q_e ($\text{g}\cdot\text{g}^{-1}$) is calculated using the following formula (Eq. (15)):

$$q_e = \frac{g_t - g_0 - g_b}{g_0} \quad (15)$$

Here, q_e represents the adsorption capacity per gram of adsorbent at a given time (min), g_t and g_0 are the post-adsorption and initial weights of the vial containing the adsorbent, respectively, and g_b is the weight of the blank reference vial.

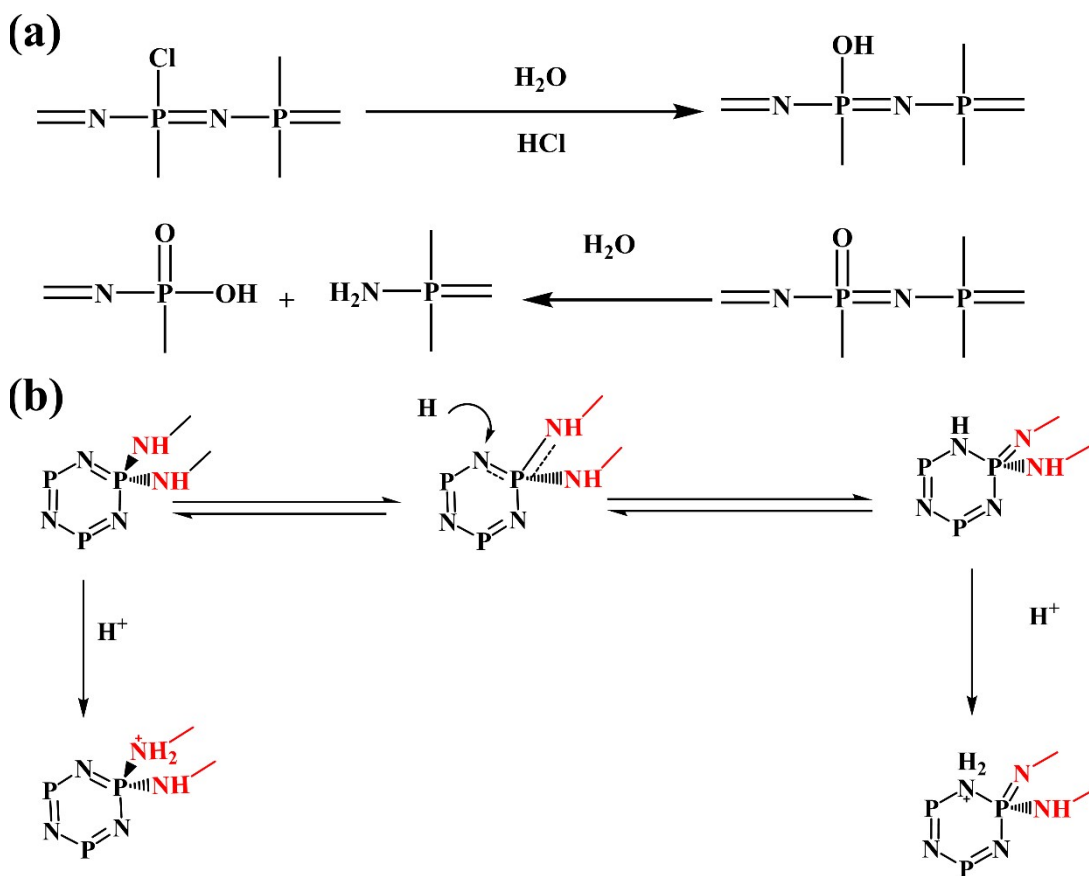
The adsorbed materials were immersed in ethanol at 348.15 K, with the ethanol solution being replaced continuously until the solution became clear. The materials were then dried and the process was repeated six times to determine the adsorption recycling efficiency.

Iodine Water Recycling Experiment: 10 mg of adsorbent was added to 100 mL of a 100 mg L^{-1} iodine solution, and the mixture was stirred at room temperature for 48 h. Afterward, samples were taken, and the residual iodine concentration in the solution was measured using a UV-Vis spectrophotometer. The removal efficiency E (%) of the adsorbent for iodine in the water was calculated using the following formula (Eq. (16)):

$$q_e = \frac{g_t - g_0 - g_b}{g_0} \quad (16)$$

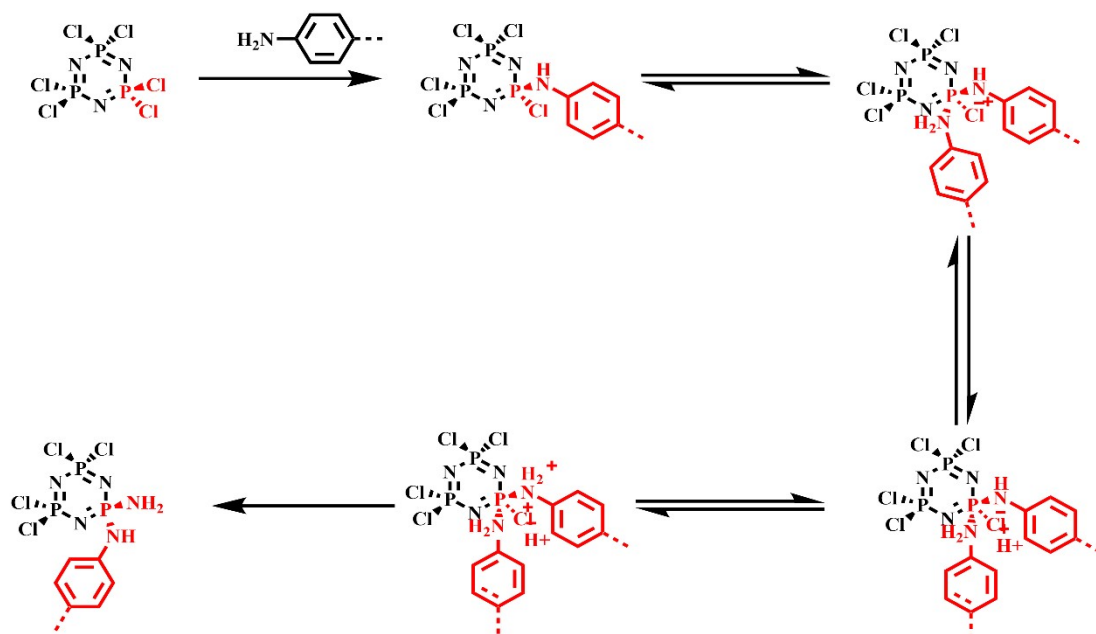
Here, q_e represents the adsorption capacity per gram of adsorbent at a given time (min), g_t and g_0 are the post-adsorption and initial weights of the vial containing the adsorbent, respectively, and g_b is the weight of the blank reference vial.

Scheme S1 Synthesis route of X-HCCP.



Scheme S1 The structural resonance and protonation of amino or phosphazene ring nitrogen.

Scheme S2 Synthesis route of TAPA-HCCP and TAPDA-HCCP.



Scheme S2 The reversible spatial isomerization mechanism used for the polymerization of TAPA-HCCP and TAPDA-HCCP.

Fig. S1 FT-IR spectroscopy.

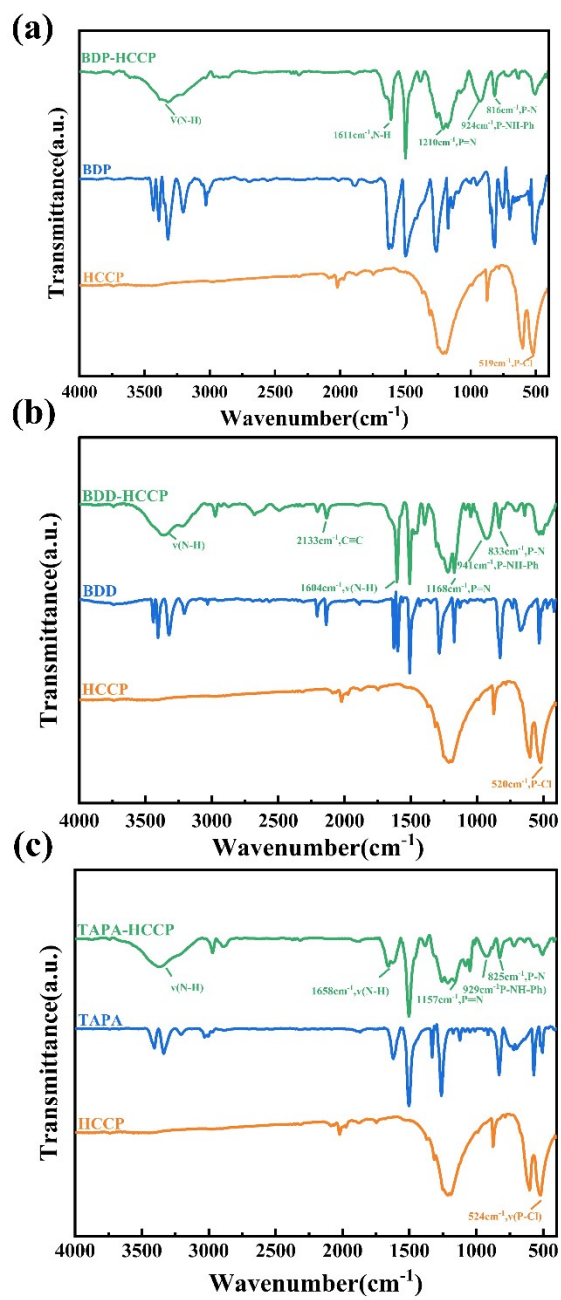


Fig. S1 FT-IR spectroscopy of (a) BDP-HCCP (b) BDD-HCCP (c) TAPDA-HCCP.

Fig. S2 XRD patterns.

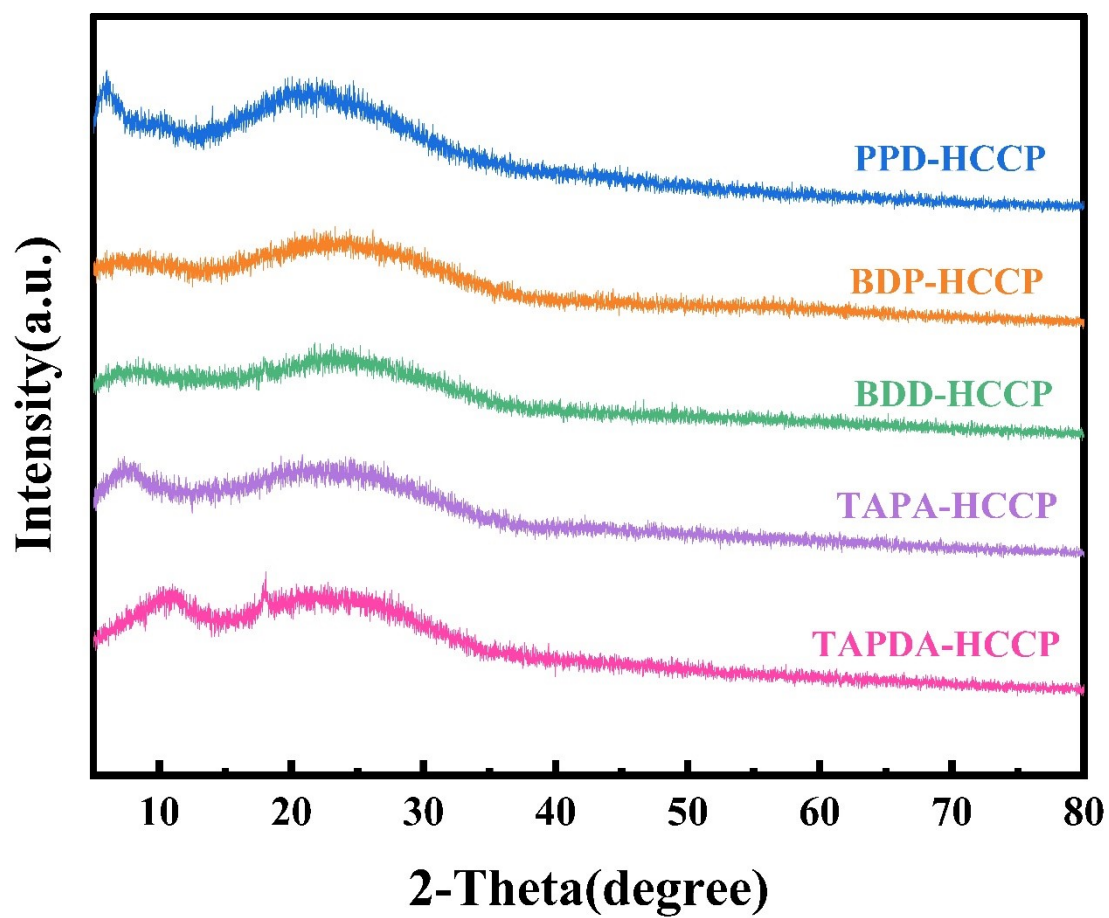


Fig. S2 XRD patterns of phosphonitrilic polymers.

Fig. S3 XPS spectra of N1s.

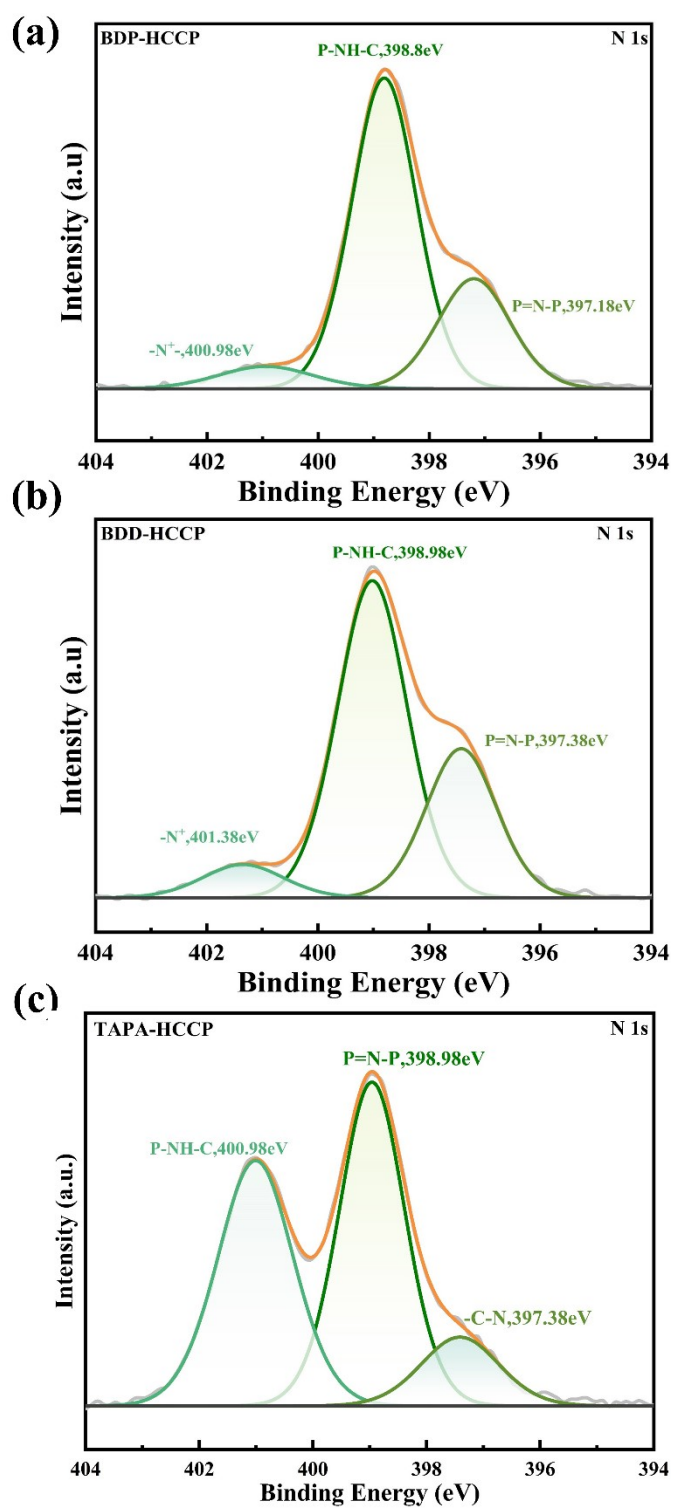


Fig. S3 XPS spectra of N1s for (a) BDP-HCCP (b) BDD-HCCP (c) TAPDA-HCCP.

Fig. S4 SEM images.

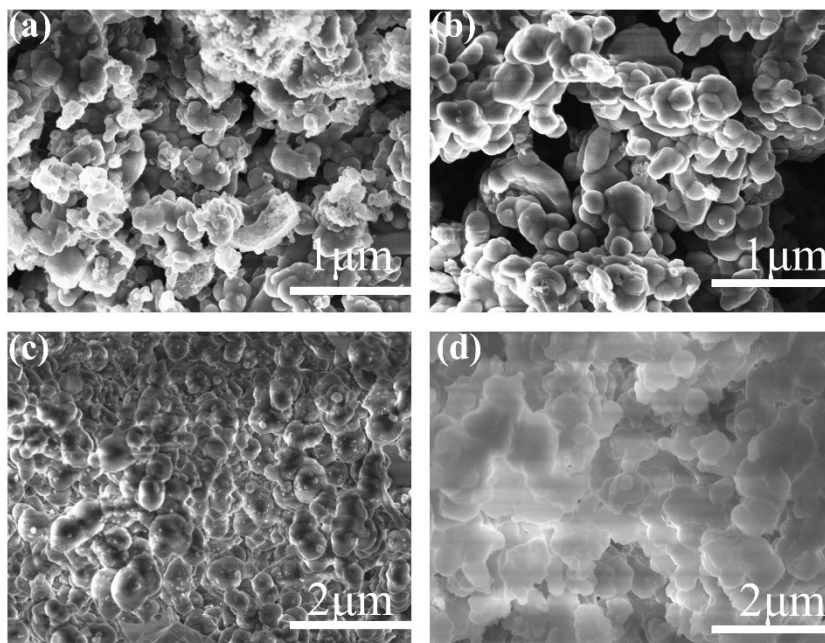


Fig. S4 SEM images of (a) and (b) BDP-HCCP, (c) and (d) BDD-HCCP.

Fig. S5 TGA curve.

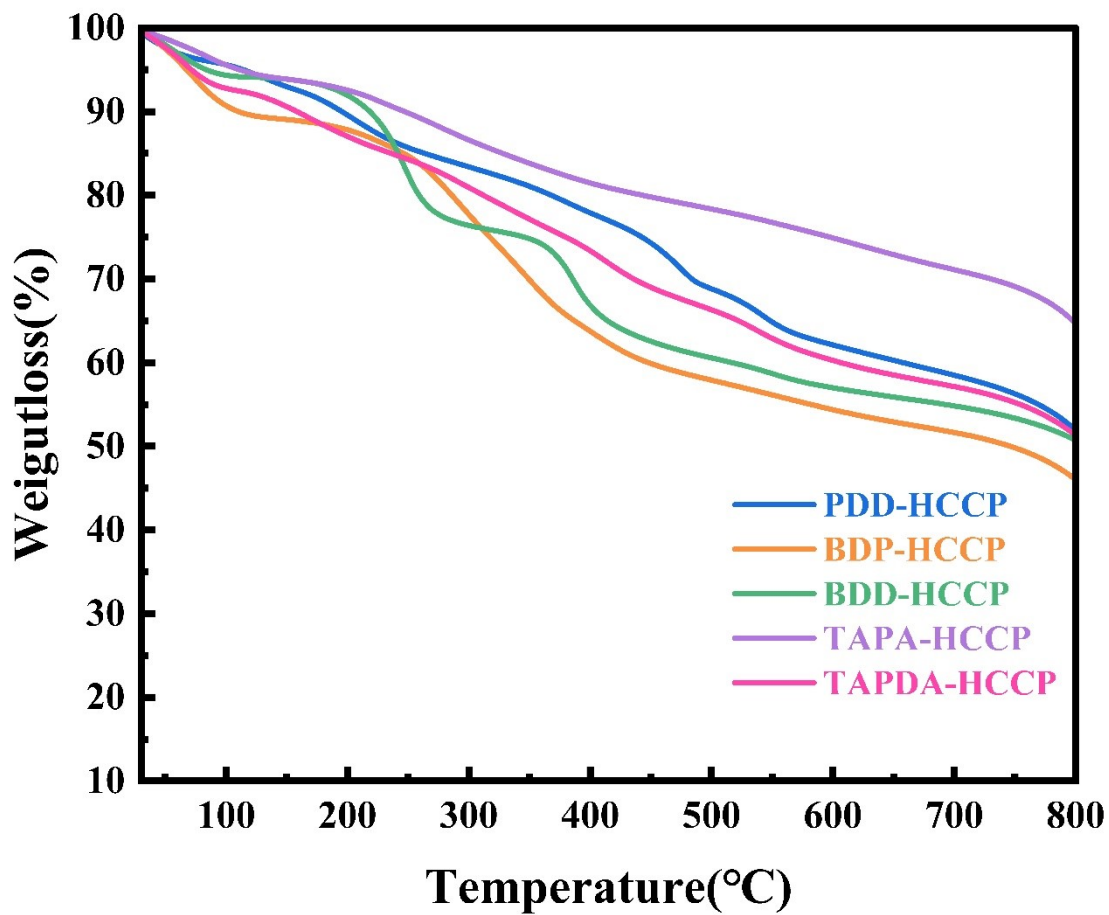


Fig. S5 TGA curve of phosphonitrilic polymers.

Fig. S6 N₂ adsorption-desorption isotherms and pore size distribution

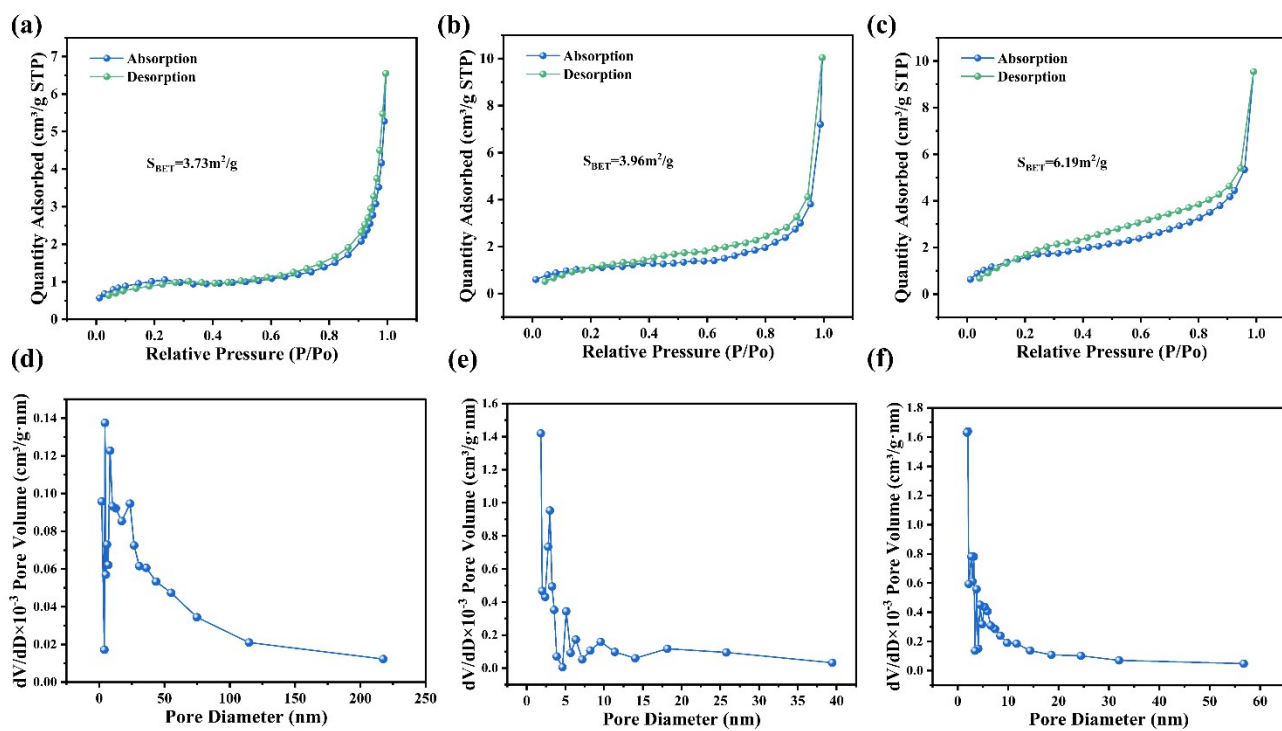


Fig. S6 N₂ adsorption-desorption isotherms of PDD-HCCP (a), BDD-HCCP (b) and TAPDA-HCCP (c). Pore size distribution of PDD-HCCP (d), BDD-HCCP (e) and TAPDA-HCCP (f).

Fig. S7 Color change of materials.

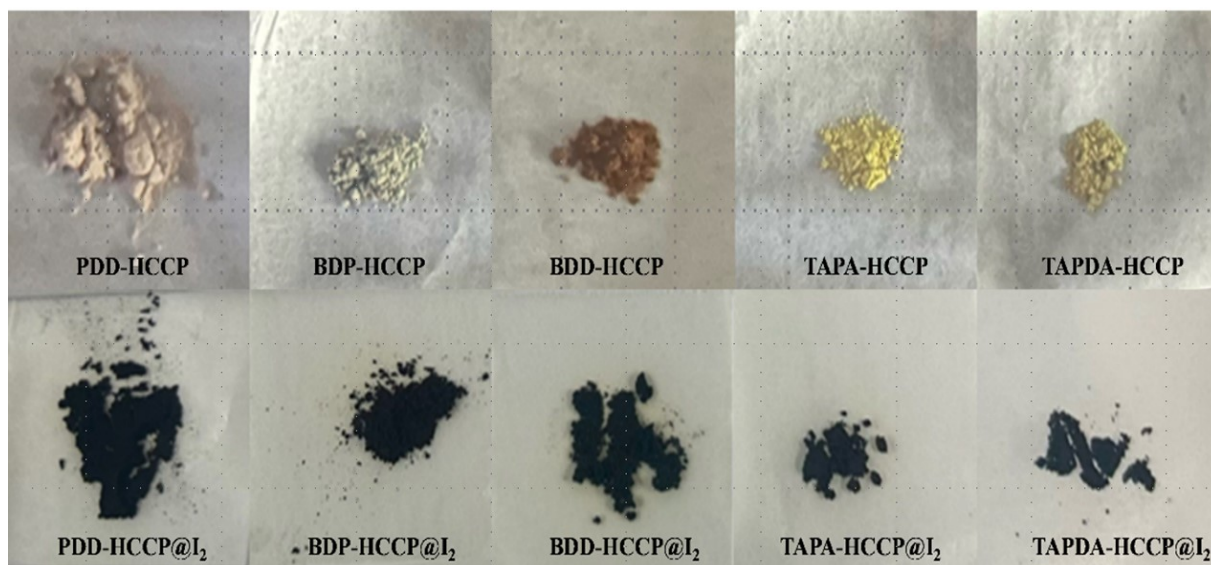


Fig. S7 Visual observation of color changes in phosphonitrilic polymers upon iodine adsorption.

Fig. S8 Summary of the I₂ vapor adsorption performance.

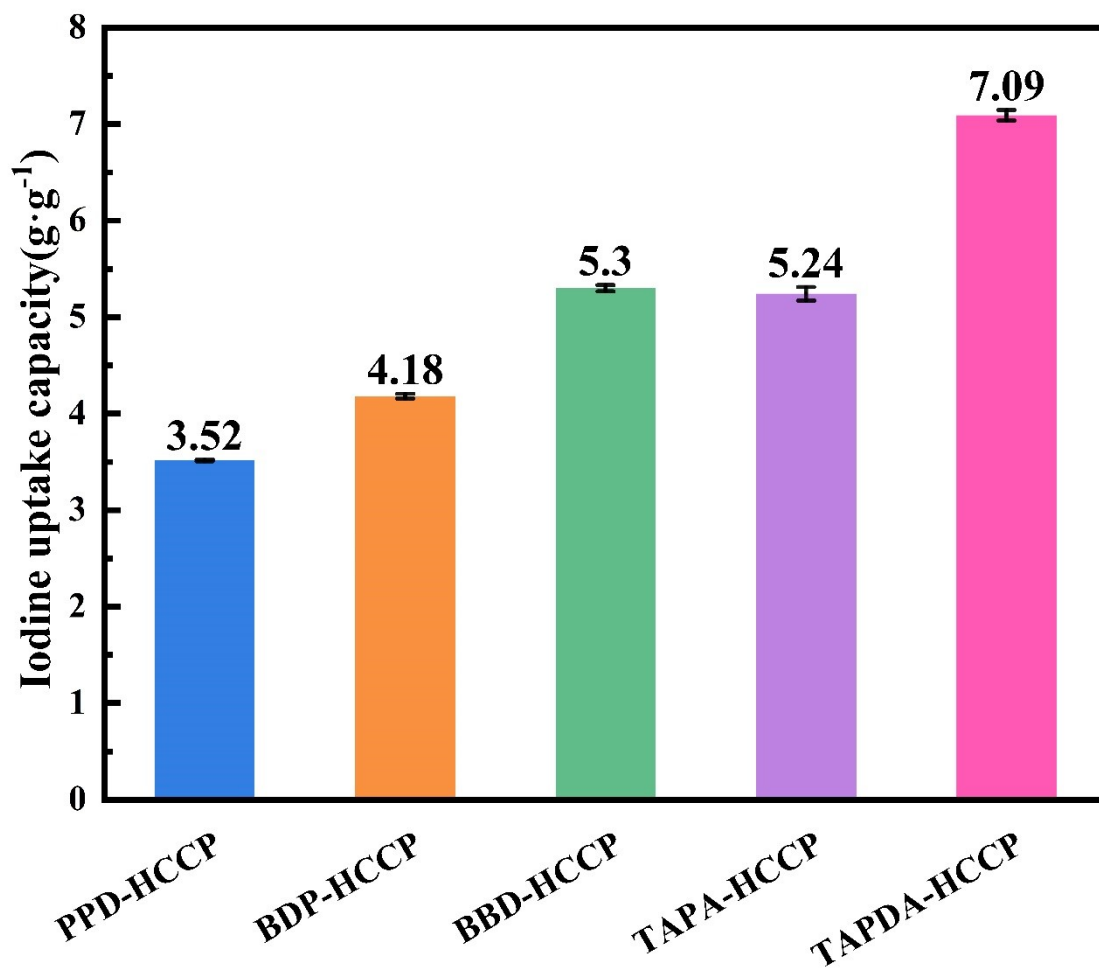


Fig. S8. Summary of the I₂ vapor adsorption performance of phosphonitrilic polymers.

Fig. S9 Kinetic model diagram of iodine vapor adsorption.

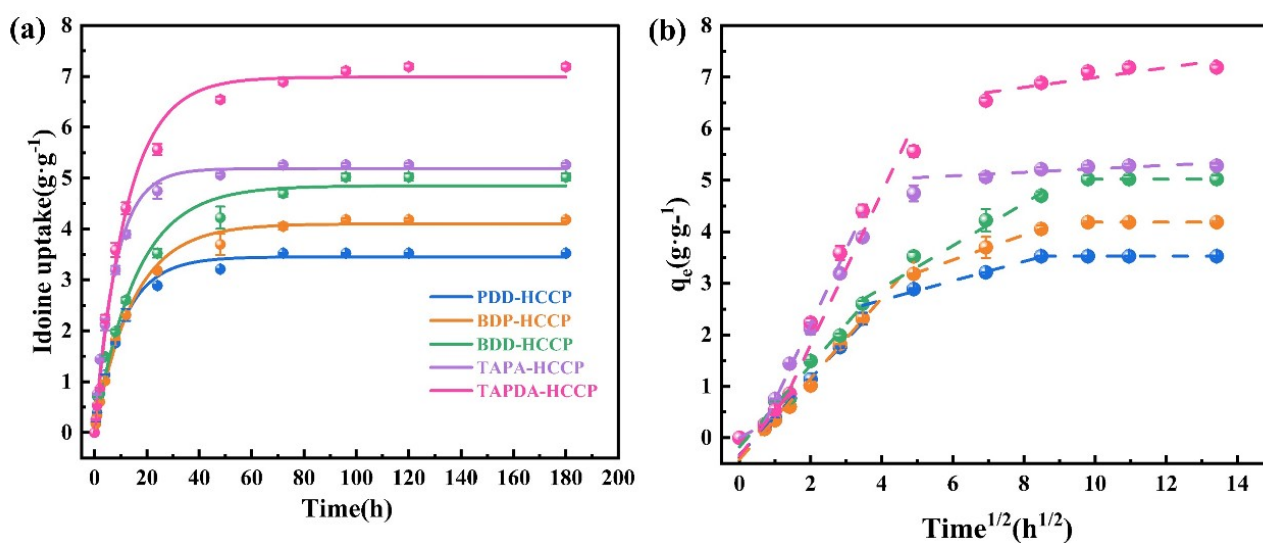


Fig. S9 Kinetic model diagram of iodine vapor adsorption. (a) Pseudo-first-order kinetic model fit for iodine vapor adsorption of phosphonitrilic polymers. (b) Weber and Morris intraparticle diffusion kinetics for uranium adsorption on three POPs.

Fig. S10 The color change of iodine solution.

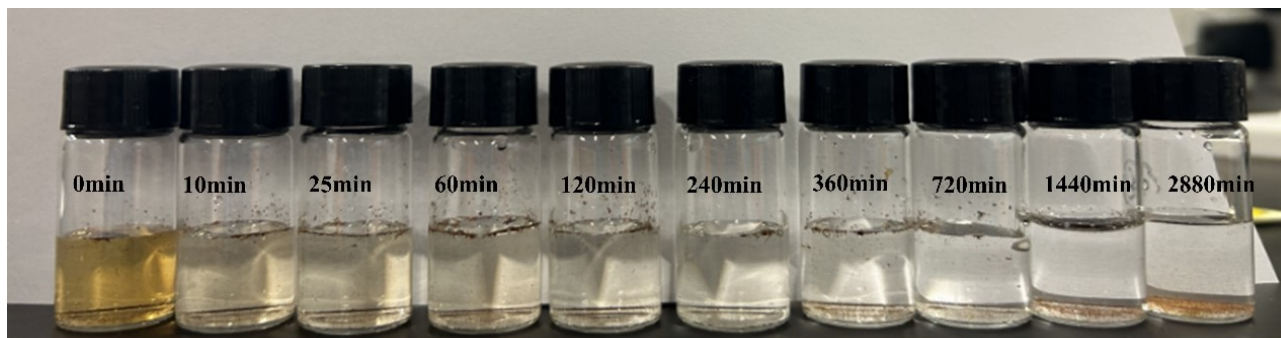


Fig. S10 The color change chart of iodine solution.

Fig. S11 Water contact angle diagram.

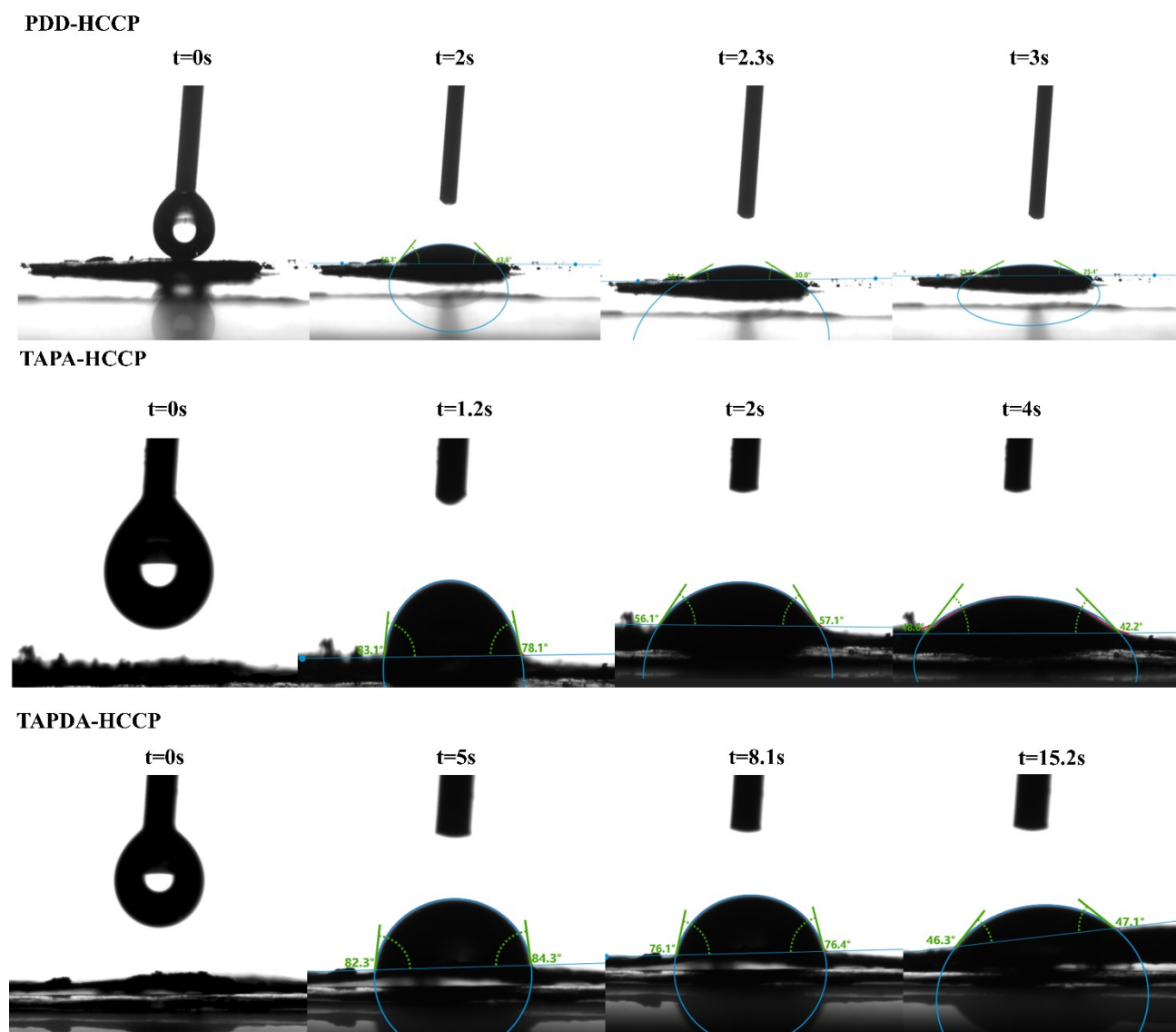


Fig. S11 The snapshots of water contact angle test of Phosphonitrilic Polymers.

Fig. S12 The first-order kinetic model of iodine solution and the Freundlich model.

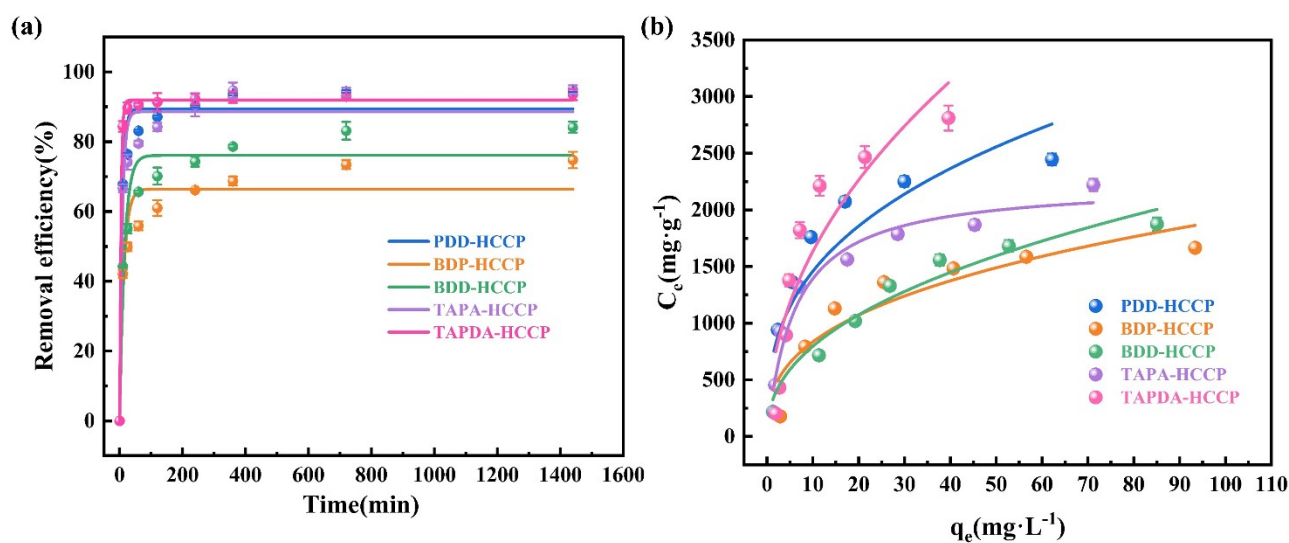


Fig. S12 The first-order kinetic model of iodine solution and the Freundlich model. (a) Pseudo-first-order kinetic model fit for iodine water absorption of Phosphonitrilic Polymers. (b) Adsorption isotherm of PDD-HCCP, BDP-HCCP, BDD-HCCP, TAPA-HCCP, TAPDA-HCCP with Freundlich isotherm model fitting for experimental data.

Fig. S13 Comparison chart of iodine water properties.

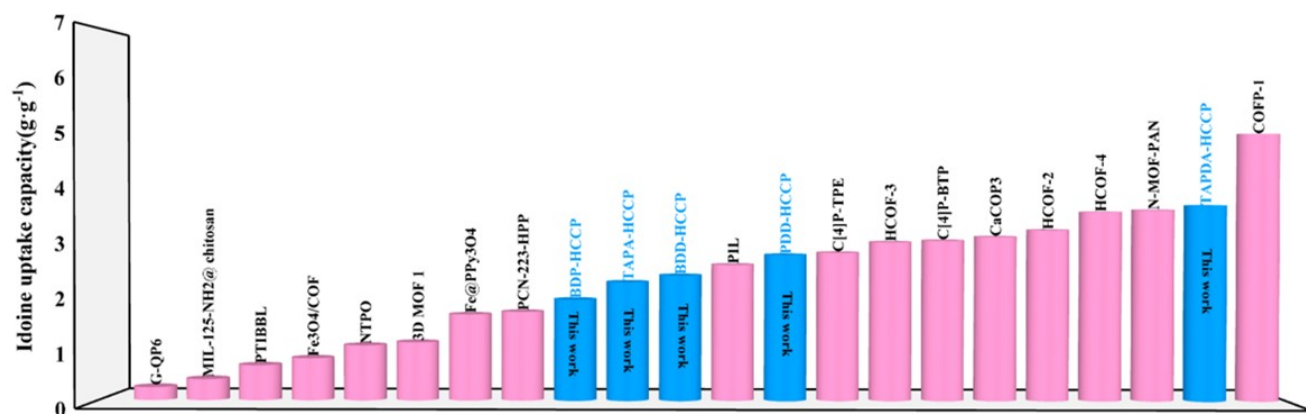


Fig. S13 Comparison of iodine adsorption in water.

Fig. S14 Kinetic model of iodine ion adsorption.

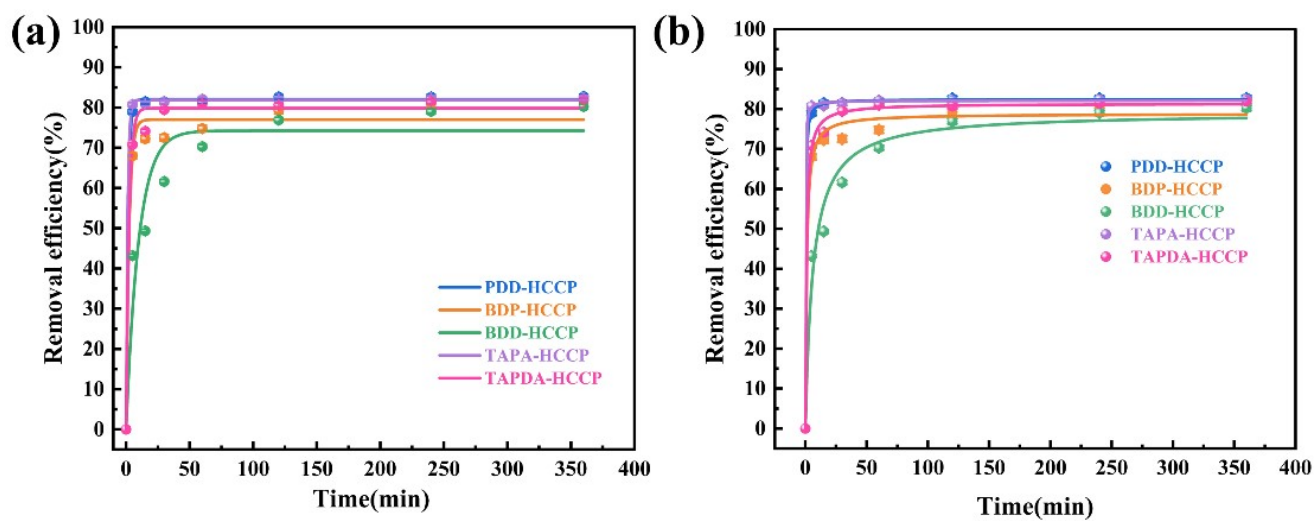


Fig. S14 (a) Pseudo-first-order and (b) Pseudo-second-order Kinetics of Iodine Ions.

Fig. S15 The first-order kinetic model and Freundlich model of methyl iodide and iodocyclohexane.

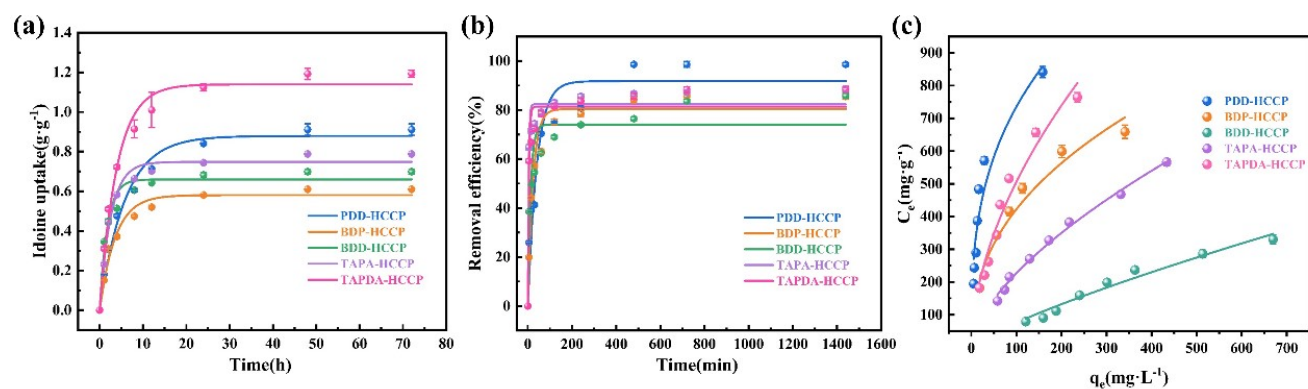


Fig. S15 (a) Pseudo-first-order kinetic model fit for Methyl Iodide absorption of Phosphonitrilic Polymers. (b) Pseudo-first-order kinetic model fit for iodocyclohexane absorption of Phosphonitrilic Polymers. (c) Freundlich adsorption isotherm model for iodine in cyclohexane on PDD-HCCP, BDP-HCCP, BDD-HCCP, TAPA-HCCP, and TAPDA-HCCP.

Fig. S16 Adsorption penetration curve.

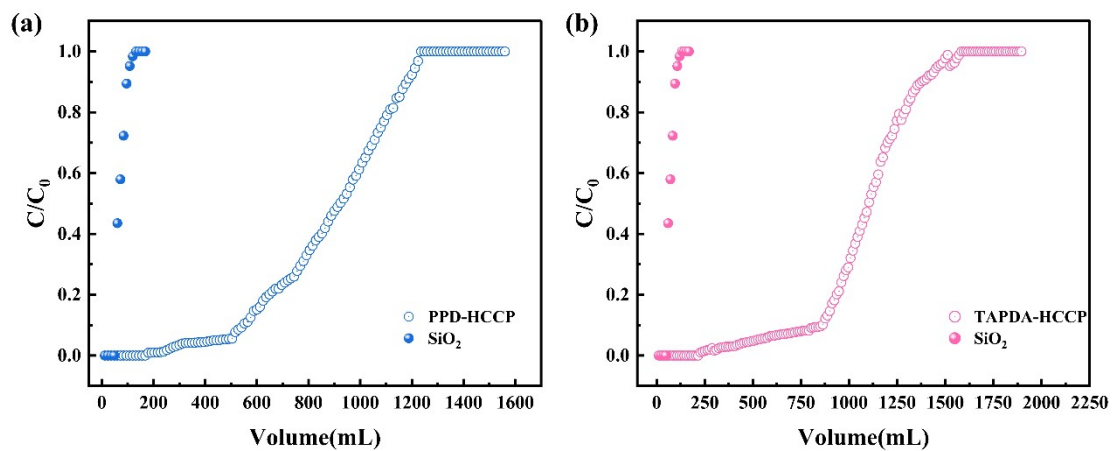


Fig. S16 (a) The iodine-water penetration curve of PDD-HCCP. (b) The iodine-water penetration curve of TAPDA-HCCP.

Fig. S17 Iodine vapor and iodine water reusability experiment.

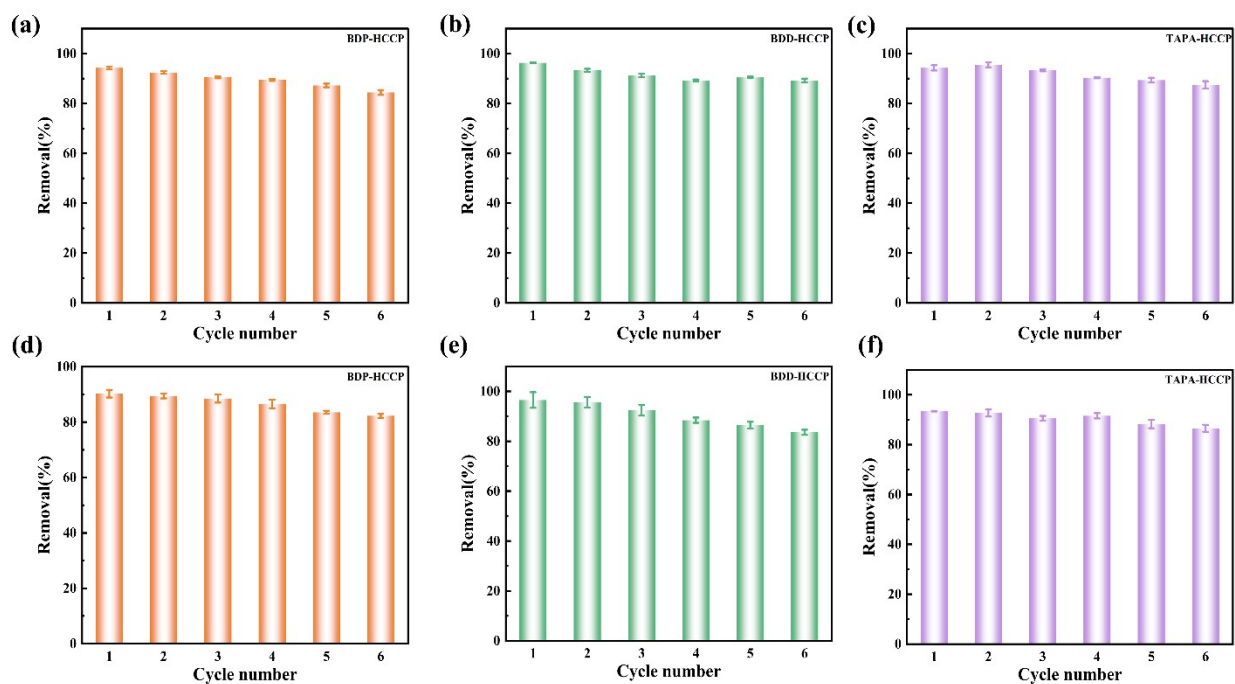


Fig. S17 Reusability study over 6 consecutive cycles in iodine vapour of (a) BDP-HCCP, (b) BDD-HCCP, and (c) TAPA-HCCP and in iodine water of (d) BDP-HCCP, (e) BDD-HCCP, and (f) TAPA-HCCP.

Fig. S18 Methyl iodide reusability experiment.

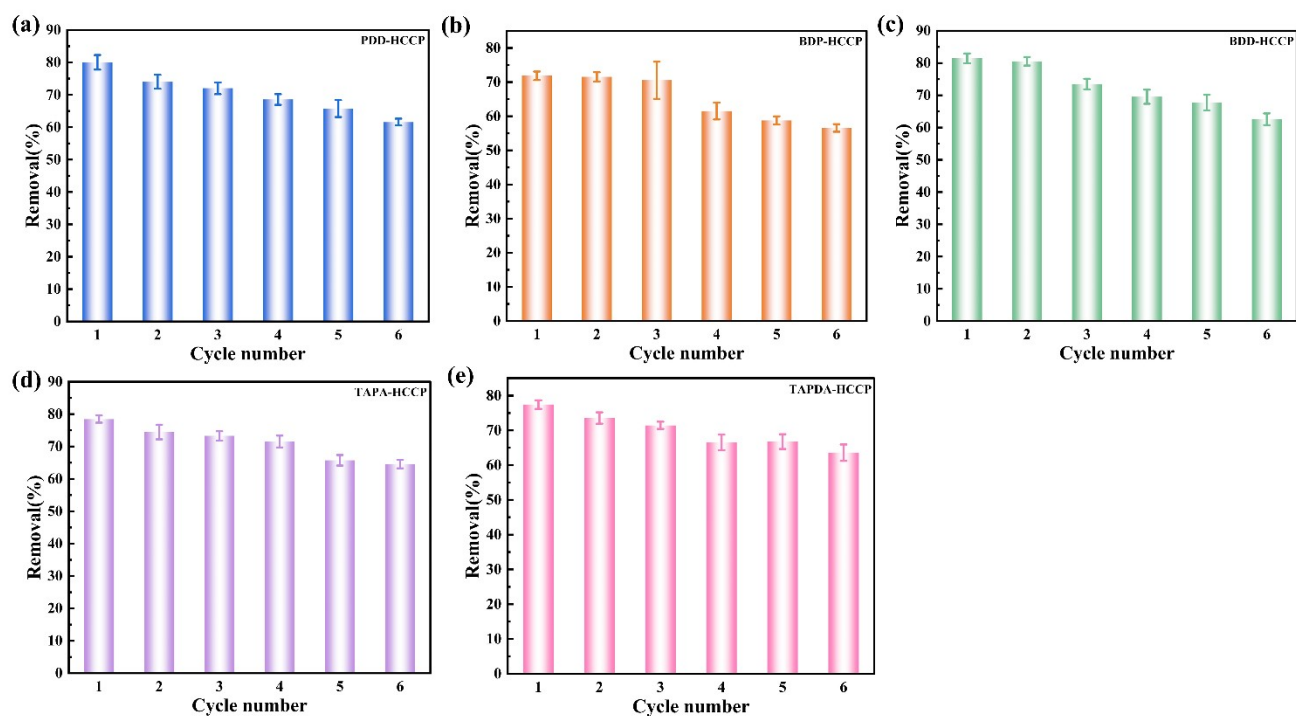


Fig. S18 Reusability study over 6 consecutive cycles in methyl iodide of (a) PDD-HCCP, (b) BDP-HCCP, (c) BDD-HCCP, (d) TAPA-HCCP, (e) TAPDA-HCCP.

Fig. S19 FT-IR spectra before and after iodine vapor adsorption.

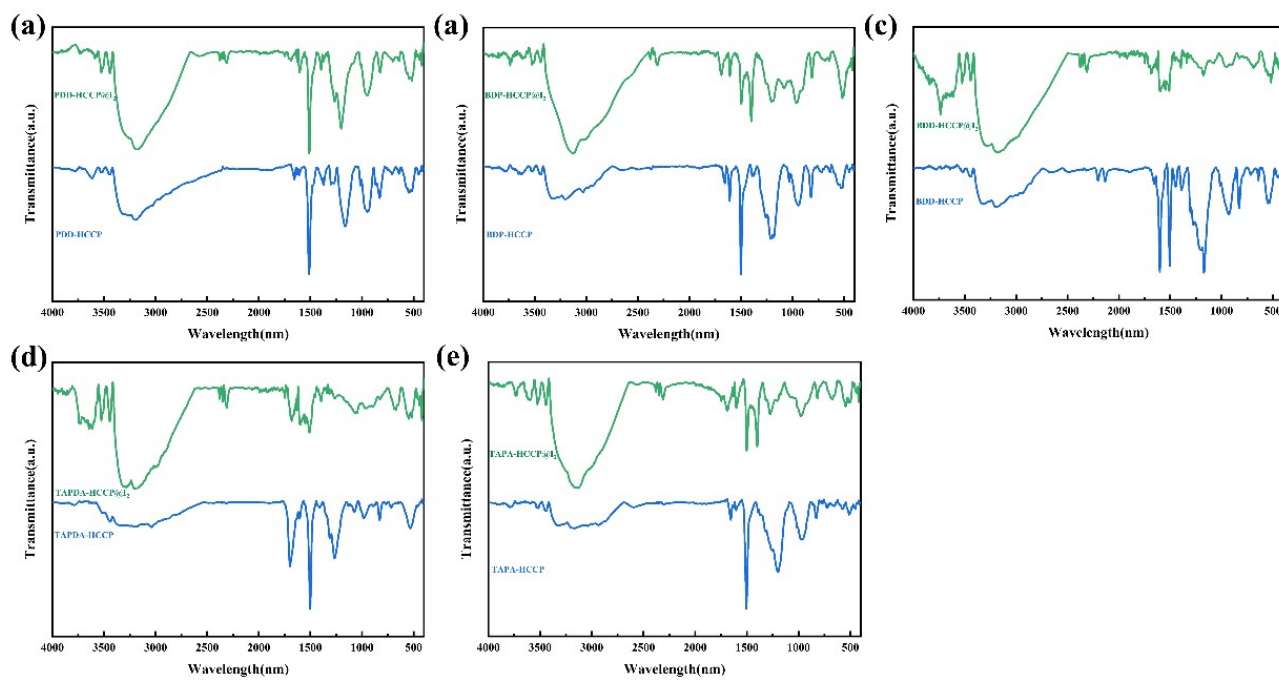


Fig. S19 FT-IR spectrum after iodine adsorption of (a)PDD-HCCP, (b)BDP-HCCP, (c)BDD-HCCP, (d)TAPA-HCCP, and (e)TAPDA-HCCP.

Fig. S20 XPS spectrum of BDD-HCCP.

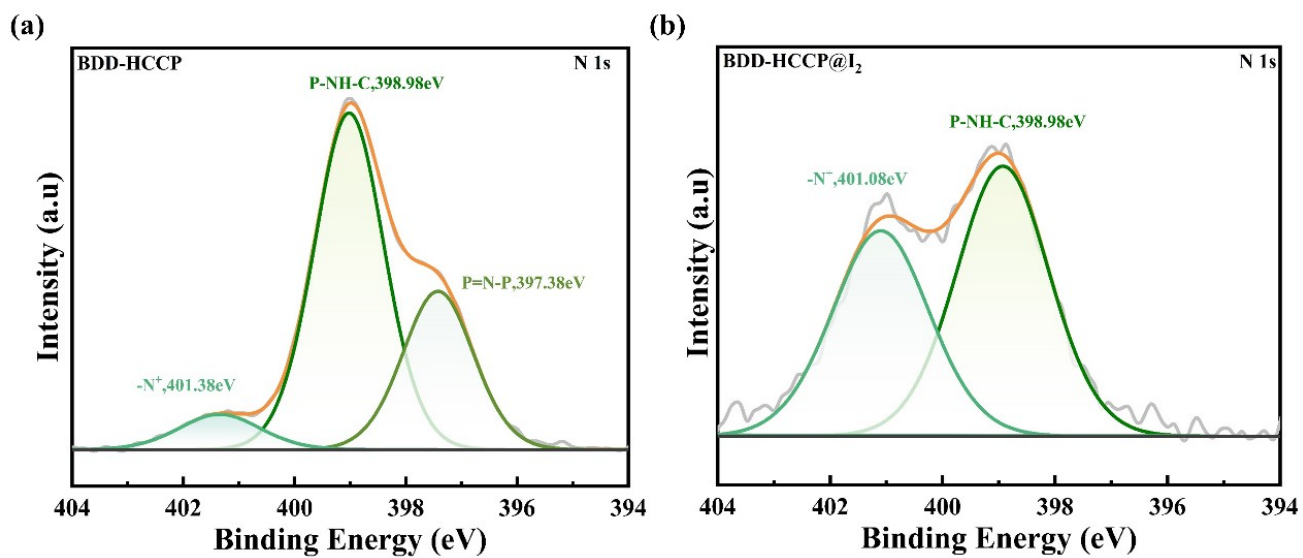


Fig. S20 XPS spectrum of N1s for BDD-HCCP (a) before and (b) after iodine vapor adsorption.

Fig. S21 XPS spectra of P 2p.

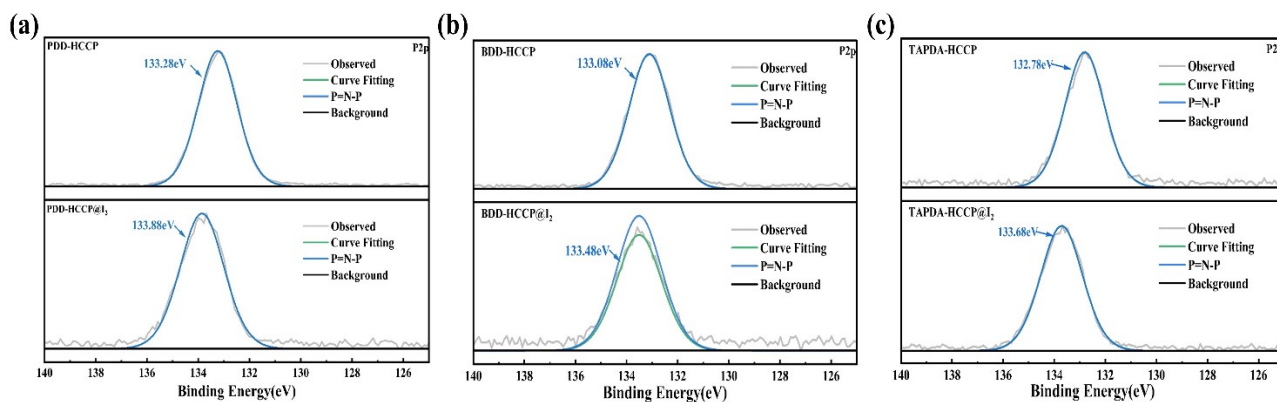


Fig. S21 (a) PDD-HCCP, (b) BDD-HCCP, and (c) TAPDA-HCCP before and after iodine vapor adsorption.

Table of experimental dates and other information.

Table S1 Yield of phosphazene polymers synthesized at different condition.

Materials	Time(h)	Temperature (°C)	Productivity(%)
PDD-HCCP	6	85	84.6
	12	85	88.8
	24	85	90.1
BDP-HCCP	6	85	82.2
	12	85	86.1
	24	85	89.1
BDD-HCCP	6	85	69.3
	12	85	83.5
	24	85	86.8
TAPA-HCCP	6	85	72.2
	12	85	75.8
	24	85	81.3
TAPDA-HCCP	6	85	78.2
	12	85	81.4
	24	85	83.5

Table S2 Idoine vapor adsorption capacity comparison of five phosphazene polymer and reported adsorbents.

Type	Materials	Iodine vapour absorption	Refs	
COFs	iCOF-AB-50	10.21	1	
	QTD-COF-V	6.29	2	
	TJNU-201	5.62	3	
	SIOC-COF-7	4.81	4	
	IL@PCN-333 (Al)	7.35	5	
MOFs	HKUST-1@PES	5.38	6	
	PCN-333 (Al)	4.42	5	
	N-MOF-PAN fibers	3.20	7	
	NH ₂ -MIL-101-on-NH ₂ -UiO-66	1.93	8	
	BisImi-POP@2	10.3	9	
POPs	BisImi-POP@1	9.5	9	
	EtAn[2]	7.35	10	
	TAPDA-HCCP	7.09	This work	
	MeAn[2]	7.01	10	
	60PEI@HCP	6.07	11	
	Δ@PPG6	6.00	12	
	C-poly-1 ₅	5.74	13	
	BDD-HCCP	5.30	This work	
	TAPA-HCCP	5.24	This work	
	BDP-HCCP	4.18	This work	
	PDD-HCCP	3.51	This work	
	C[4]P-BTP	3.38	14	
	C[4]P-HEPM	3.18	15	
	Other	SCU-SnS	6.12	16
		SnSg	0.68	17
Si-BEA		0.47	18	

Table S3 Comparison of iodine vapor adsorption performance of various porous materials

Adsorbents	$K_{80\%}$	Saturation time (h)	Iodine capacity($\text{g}\cdot\text{g}^{-1}$)	Refer
TAPA-HCCP	0.256	72	5.26	This work
TJNU-201	0.225	25	5.63	³
TAPDA-HCCP	0.201	96	7.19	This work
TPE-TAPD-CMP	0.19	20	4.68	¹⁹
Th-SINAP-8	0.19	3	0.47	²⁰
MOF-808	0.15	20	2.18	²¹
ZIF-90	0.15	24	4.49	²²
PDD-HCCP	0.124	72	3.53	This work
BDP-HCCP	0.106	96	4.19	This work
BDD-HCCP	0.098	96	5.02	This work
$[\text{Zn}_2(\text{tpc})-(\text{apy})_2\cdot x(\text{H}_2\text{O})_x]\cdot \text{H}_2\text{O}$	0.07	50	2.16	²³

Table S4 Kinetics parameters for Idoine vapour extraction of PDD-HCCP, BDP-HCCP, BDD-HCCP, TAPA-HCCP, and TAPDA-HCCP.

Sample	Pseudo-first-order		Pseudo-second-order	
PDD-HCCP	K_1 (h^{-1})	0.091	K_2 (g (g/h) $^{-1}$)	0.031
	q_e ($g \cdot g^{-1}$)	3.453	q_e ($mg \cdot g^{-1}$)	3.809
	R^2	0.997	R^2	0.999
BDP-HCCP	K_1 (h^{-1})	0.070	K_2 (g (g/h) $^{-1}$)	0.018
	q_e ($g \cdot g^{-1}$)	4.101	q_e ($mg \cdot g^{-1}$)	4.640
	R^2	0.998	R^2	0.999
BDD-HCCP	K_1 (h^{-1})	0.068	K_2 (g (g/h) $^{-1}$)	0.017
	q_e ($g \cdot g^{-1}$)	4.850	q_e ($mg \cdot g^{-1}$)	5.485
	R^2	0.992	R^2	0.997
TAPA-HCCP	K_1 (h^{-1})	0.124	K_2 (g (g/h) $^{-1}$)	0.030
	q_e ($g \cdot g^{-1}$)	5.187	q_e ($mg \cdot g^{-1}$)	5.618
	R^2	0.997	R^2	0.998
TAPDA-HCCP	K_1 (h^{-1})	0.081	K_2 (g (g/h) $^{-1}$)	0.013
	q_e ($g \cdot g^{-1}$)	6.986	q_e ($g \cdot g^{-1}$)	7.828
	R^2	0.997	R^2	0.998

Table S5 Weber and Morris intraparticle diffusion kinetics for iodine vapor adsorption on five Phosphonitrilic Polymers.

Sample				
	K (g·g⁻¹·h^{1/2})	0.740	0.188	0
PDD-HCCP	C	-0.329	1.915	3.525
	R²	0.994	0.984	0.999
	K (g·g⁻¹·h^{1/2})	0.781	0.243	4.185
BDP-HCCP	C	-0.417	1.990	-3.49
	R²	0.991	0.999	1
	K (g·g⁻¹·h^{1/2})	0.792	0.412	5.024
BDD-HCCP	C	-0.175	1.257	0
	R²	0.903	0.981	1
	K (g·g⁻¹·h^{1/2})	0.372	1.461	0.031
TAPA-HCCP	C	5.5×10 ⁻¹⁷	-0.729	5.021
	R²	1	0.985	0.891
	K (g·g⁻¹·h^{1/2})	0.866	1.473	0.096
TAPDA-HCCP	C	-0.349	-1.139	6.136
	R²	0.998	0.966	0.897

Table S6 Comparison of iodine water adsorption performance of various porous materials

Adsorbents	K (g·g ⁻¹ ·min ⁻¹)	Refer
TAPDA-HCCP	1.10	This work
C[4]P-DPP	0.95	14
C-poly-I ₅	0.84	24
C[4]P-BT	0.67	14
C-poly-I ₂₀	0.62	24
C[4]P-TTP	0.47	14
C-poly-I ₅₀	0.39	24
PDD-HCCP	0.25	This work
TAPA-HCCP	0.23	This work
BDP-HCCP	0.15	This work
BDD-HCCP	0.12	This work
N-MOF-PAN	0.033	7
Lac-zn	0.02	25

Table S7 Kinetics parameters for iodide water extraction of PDD-HCCP, BDP-HCCP, BDD-HCCP, TAPA-HCCP, TAPDA-HCCP

Sample	Pseudo-first-order		Pseudo-second-order	
PDD-HCCP	$K_1(\text{min}^{-1})$	0.127	$K_2 (\text{g (mg/ min)}^{-1})$	2.5×10^{-4}
	$q_e (\text{mg} \cdot \text{g}^{-1})$	894.6	$q_e (\text{mg} \cdot \text{g}^{-1})$	926.5
	R^2	0.985	R^2	0.997
BDP-HCCP	$K_1(\text{min}^{-1})$	0.0762	$K_2 (\text{g (mg/ min)}^{-1})$	1.5×10^{-4}
	$q_e (\text{mg} \cdot \text{g}^{-1})$	664.5	$q_e (\text{mg} \cdot \text{g}^{-1})$	702.6
	R^2	0.960	R^2	0.986
BDD-HCCP	$K_1(\text{min}^{-1})$	0.065	$K_2 (\text{g (mg/ min)}^{-1})$	1.2×10^{-4}
	$q_e (\text{mg} \cdot \text{g}^{-1})$	761.0	$q_e (\text{mg} \cdot \text{g}^{-1})$	804.3
	R^2	0.970	R^2	0.992
TAPA-HCCP	$K_1(\text{min}^{-1})$	0.122	$K_2 (\text{g (mg/ min)}^{-1})$	2.3×10^{-4}
	$q_e (\text{mg} \cdot \text{g}^{-1})$	885.6	$q_e (\text{mg} \cdot \text{g}^{-1})$	921.5
	R^2	0.976	R^2	0.992
TAPDA-HCCP	$K_1(\text{min}^{-1})$	0.248	$K_2 (\text{g (mg/ min)}^{-1})$	1.1×10^{-3}
	$q_e (\text{mg} \cdot \text{g}^{-1})$	919.3	$q_e (\text{mg} \cdot \text{g}^{-1})$	928.5
	R^2	0.998	R^2	0.999

Table S8 Isotherm parameters for iodine water solution extraction of five phosphazene polymer

Models	Parm	Sample				
		PDD-HCCP	BDP-HCCP	BDD-HCCP	TAPA-HCCP	TAPDA-HCCP
Langmuir	Q_{\max} (mg·g ⁻¹)	2.755	1.908	2.366	2.239	3.693
	K_L (L·m·g ⁻¹)	0.161	0.088	0.046	0.165	0.099
	R^2	0.981	0.985	0.984	0.977	0.961
	1/n	0.348	0.359	0.431	0.344	0.470
Freundlich	K_f (L·g·g ⁻¹ ·g ^{1/n})	654.3	365.9	295.6	531.8	533.7
	R^2	0.919	0.941	0.983	0.946	0.911

Table S9 Idoine water solution adsorption capacity comparison of five phosphazene polymer and reported adsorbents.

Type	Materials	Iodine	Ref.
COFs	COF-TAPB	7.61	26
	COFP-1	5.05	27
	HCOF-4	3.57	27
	HCOF-2	3.23	27
	HCOF-3	3.00	27
MOFs	N-MOF-PAN	3.61	6
	PCN-233-HPP	1.67	28
	3D MOF 1	1.10	29
	MIL-125-NH ₂ @chitosan	0.41	30
	SUPE-py-Imine-Cage	7.40	31
POPs	C[4]P-BTP	3.03	14
	C[4]P-TPE	2.80	14
	CaCop3	3.10	28
	TIEPE-DABCO	1.80	32
	G-QP6	0.25	33
Other	PTIBBL	0.66	34
	PIL	2.57	35
	Fe@PPy ₃ O ₄	1.63	36
	NTPO	1.04	37

Table S10 Isotherm parameters for iodine ion solution extraction of five phosphazene polymer

Sample	Pseudo-first-order		Pseudo-second-order	
PDD-HCCP	K₁ (h⁻¹)	0.654	K₂ (g (mg/ min)⁻¹)	0.011
	q_e (mg·g⁻¹)	410.4	q_e (mg·g⁻¹)	412.4
	R²	0.998	R²	0.999
BDP-HCCP	K₁ (h⁻¹)	0.425	K₂ (g (mg/ min)⁻¹)	2.6×10 ⁻³
	q_e (mg·g⁻¹)	385.1	q_e (mg·g⁻¹)	394.1
	R²	0.991	R²	0.995
BDD-HCCP	K₁ (h⁻¹)	0.101	K₂ (g (mg/ min)⁻¹)	4.1×10 ⁻⁴
	q_e (mg·g⁻¹)	371.2	q_e (mg·g⁻¹)	395.4
	R²	0.958	R²	0.987
TAPA-HCCP	K₁ (h⁻¹)	0.852	K₂ (g (mg/ min)⁻¹)	0.024
	q_e (mg·g⁻¹)	409.4	q_e (mg·g⁻¹)	410.6
	R²	0.998	R²	0.999
TAPDA-HCCP	K₁ (h⁻¹)	0.430	K₂ (g (mg/ min)⁻¹)	2.9×10 ⁻³
	q_e (mg·g⁻¹)	399.2	q_e (mg·g⁻¹)	407.1
	R²	0.996	R²	0.999

Table S11 Kinetics parameters for methyl iodide extraction of PDD-HCCP, BDP-HCCP, BDD-HCCP, TAPA-HCCP, TAPDA-HCCP

Sample	Pseudo-first-order		Pseudo-second-order	
PDD-HCCP	K_1 (h^{-1})	0.171	K_2 (g (g/h) $^{-1}$)	0.227
	q_e ($g \cdot g^{-1}$)	0.879	q_e ($mg \cdot g^{-1}$)	0.982
	R^2	0.992	R^2	0.999
BDP-HCCP	K_1 (h^{-1})	0.278	K_2 ($g \cdot (g/h)^{-1}$)	0.591
	q_e ($g \cdot g^{-1}$)	0.581	q_e ($mg \cdot g^{-1}$)	0.638
	R^2	0.987	R^2	0.997
BDD-HCCP	K_1 (h^{-1})	0.564	K_2 (g (g/h) $^{-1}$)	1.203
	q_e ($g \cdot g^{-1}$)	0.660	q_e ($mg \cdot g^{-1}$)	0.707
	R^2	0.981	R^2	0.998
TAPA-HCCP	K_1 (h^{-1})	0.389	K_2 (g (g/h) $^{-1}$)	0.649
	q_e ($g \cdot g^{-1}$)	0.748	q_e ($mg \cdot g^{-1}$)	0.816
	R^2	0.992	R^2	0.997
TAPDA-HCCP	K_1 (h^{-1})	1.139	K_2 (g ($g \cdot h^{-1}$) $^{-1}$)	0.269
	q_e ($g \cdot g^{-1}$)	0.251	q_e ($g \cdot mg^{-1}$)	1.256
	R^2	0.991	R^2	0.999

Table S12 Kinetics parameters for iodide water extraction of PDD-HCCP, BDP-HCCP, BDD-HCCP, TAPA-HCCP, TAPDA-HCCP

Sample	Pseudo-first-order		Pseudo-second-order	
PDD-HCCP	K_1 (min^{-1})	0.127	K_2 (g (mg/ min)^{-1})	2.5×10^{-4}
	q_e ($\text{mg} \cdot \text{g}^{-1}$)	894.6	q_e ($\text{mg} \cdot \text{g}^{-1}$)	926.5
	R^2	0.985	R^2	0.997
BDP-HCCP	K_1 (min^{-1})	0.0762	K_2 ($\text{g (mg} \cdot \text{min)}^{-1}$)	1.5×10^{-4}
	q_e ($\text{mg} \cdot \text{g}^{-1}$)	664.5	q_e ($\text{mg} \cdot \text{g}^{-1}$)	702.6
	R^2	0.960	R^2	0.986
BDD-HCCP	K_1 (min^{-1})	0.065	K_2 (g (mg/ min)^{-1})	1.2×10^{-4}
	q_e ($\text{mg} \cdot \text{g}^{-1}$)	761.0	q_e ($\text{mg} \cdot \text{g}^{-1}$)	804.3
	R^2	0.970	R^2	0.992
TAPA-HCCP	K_1 (min^{-1})	0.122	K_2 (g (mg/ min)^{-1})	2.3×10^{-4}
	q_e ($\text{mg} \cdot \text{g}^{-1}$)	885.6	q_e ($\text{mg} \cdot \text{g}^{-1}$)	921.5
	R^2	0.976	R^2	0.992
TAPDA-HCCP	K_1 (min^{-1})	0.248	K_2 (g (mg/ min)^{-1})	1.1×10^{-3}
	q_e ($\text{mg} \cdot \text{g}^{-1}$)	919.3	q_e ($\text{mg} \cdot \text{g}^{-1}$)	928.5
	R^2	0.998	R^2	0.999

Table 13 Isotherm parameters for iodine cyclohexane extraction of five phosphazene polymer

Models	Parm	Sample				
		PDD-HCCP	BDP-HCCP	BDD-HCCP	TAPA-HCCP	TAPDA-HCCP
Langmuir	Q_{\max} ($\text{mg}\cdot\text{g}^{-1}$)	943.3	813.9	958.0	974.9	1150.4
	K_L ($\text{L}\cdot\text{m}\cdot\text{g}^{-1}$)	0.053	0.013	0.001	0.003	0.009
	R^2	0.995	0.998	0.990	0.997	0.992
	$1/n$	0.336	0.416	0.798	0.625	0.546
Freundlich	K_f ($\text{L}\cdot\text{g}\cdot\text{g}^{-1}\cdot\text{g}^{-1/n}$)	156.2	62.31	1.929	12.75	41.03
	R^2	0.970	0.982	0.985	0.994	0.955

References

1. G. Gong, J. Zhao, Y. Chen, F. Xie, F. Lu, J. Wang, L. Wang and S. Chen, An amino-type halogen-bonded organic framework for the selective adsorption of aliphatic acid vapors: insight into the competitive interactions of halogen bonds and hydrogen bonds, *J. Mater. Chem. A*, 2022, **10**, 10586-10592.
2. X. Guo, Y. Li, M. Zhang, K. Cao, Y. Tian, Y. Qi, S. Li, K. Li, X. Yu and L. Ma, Colyliform Crystalline 2D Covalent Organic Frameworks (COFs) with Quasi-3D Topologies for Rapid I₂ Adsorption, *Angew. Chem. Int. Ed*, 2020, **59**, 22697-22705.
3. J. Li, H. Zhang, L. Zhang, K. Wang, Z. Wang, G. Liu, Y. Zhao and Y. Zeng, Two-dimensional covalent-organic frameworks for ultrahigh iodine capture, *J. Mater. Chem. A*, 2020, **8**, 9523-9527.
4. Z. Yin, S. Xu, T. Zhan, Q. Qi, Z. Wu and X. Zhao, Ultrahigh volatile iodine uptake by hollow microspheres formed from a heteropore covalent organic framework, *Chem. Commun.*, 2017, **53**, 7266-7269.
5. Y. Tang, H. Huang, J. Li, W. Xue and C. Zhong, IL-induced formation of dynamic complex iodide anions in IL@MOF composites for efficient iodine capture, *J. Mater. Chem. A*, 2019, **7**, 18324-18329.
6. S. Kolay, A. K. Sahu, P. Jha, R. K. Sharma, Jagannath and R. Mishra, Capture of volatile I₂ by dithioglycol functionalized HKUST-1 and its polymeric composite beads, *J. Solid State Chem.*, 2023, **324**, 124080.
7. D. Chen, T. Ma, X. Zhao, X. Jing, R. Zhao and G. Zhu, Multi-Functionalization Integration into the Electrospun Nanofibers Exhibiting Effective Iodine Capture from Water, *ACS Appl. Mater*, 2022, **14**, 47126-47135.
8. L. Liu, L. Chen, K. Thummavichai, Z. Ye, Y. Wang, T. Fujita and X. Wang, Amino-functionalized MOF-on-MOF architectural nanocomplexes composed for radioactive-iodine efficient adsorption, *Chem. Eng. J.*, 2023, **474**, 145858.
9. T.H. Niu, C.-C. Feng, C. Yao, W.-Y. Yang and Y.-H. Xu, Bisimidazole-Based Conjugated Polymers for Excellent Iodine Capture, *ACS Applied Polymer Materials*, 2021, **3**, 354-361.
10. P. Jin, W. Liang, Y. Rong, W. Wu, M. Gou, Y. Tang and C. Yang, Remarkable iodine uptake by aniline-based macrocyclic arenes through a reverse dissolution mechanism, *J. Mater. Chem. A*, 2023, **11**, 11126-11132.
11. X. Li, G. Chen and Q. Jia, Highly efficient iodine capture by task-specific polyethylenimine impregnated hypercrosslinked polymers, *J. Taiwan Inst. Chem. Eng.*, 2018, **93**, 660-666.

12. B. T. Benkhaled, A. Chaix, C. Gomri, S. Buys, N. Namar, N. Sehoulia, R. Jadhav, J. Richard, L. Lichon, C. Nguyen, M. Gary-Bobo and M. Semsarilar, Novel Biocompatible Trianglamine Networks for Efficient Iodine Capture, *ACS Appl. Mater.*, 2023, **15**, 42942-42953.
13. X. Xu, Y. Li, L. Zhou, N. Liu and Z.-Q. Wu, Precise fabrication of porous polymer frameworks using rigid polyisocyanides as building blocks: from structural regulation to efficient iodine capture, *Chem. Sci.*, 2022, **13**, 1111-1118.
14. L. Xie, Z. Zheng, Q. Lin, H. Zhou, X. Ji, J. L. Sessler and H. Wang, Calix[4]pyrrole-based Crosslinked Polymer Networks for Highly Effective Iodine Adsorption from Water, *Angew. Chem. Int. Ed.*, 2022, **61**, e202113724.
15. Z. Zheng, Q. Lin, L. Xie, X. Chen, H. Zhou, K. Lin, D. Zhang, X. Chi, J. L. Sessler and H. Wang, Macrocyclic polymeric networks based on a chair-like calix[4]pyrrole for the rapid and efficient adsorption of iodine from water, *J. Mater. Chem. A*, 2023, **11**, 13399-13408.
16. Y. Zhang, L. He, T. Pan, J. Xie, F. Wu, X. Dong, X. Wang, L. Chen, S. Gong, W. Liu, L. Kang, J. Chen, L. Chen, L. Chen, Y. Han and S. Wang, Superior Iodine Uptake Capacity Enabled by an Open Metal-Sulfide Framework Composed of Three Types of Active Sites, *CCS Chem*, 2022, **5**, 1540-1548.
17. B. J. Riley, D. A. Pierce, J. Chun, J. Matyáš, W. C. Lepry, T. G. Garn, J. D. Law and M. G. Kanatzidis, Polyacrylonitrile-Chalcogel Hybrid Sorbents for Radioiodine Capture, *Environ. Sci. Technol.*, 2014, **48**, 5832-5839.
18. T. C. T. Pham, S. Docao, I. C. Hwang, M. K. Song, D. Y. Choi, D. Moon, P. Oleynikov and K. B. Yoon, Capture of iodine and organic iodides using silica zeolites and the semiconductor behaviour of iodine in a silica zeolite, *Energy Environ. Sci.*, 2016, **9**, 1050-1062.
19. S. Luo, Q. Yan, S. Wang, H. Hu, S. Xiao, X. Su, H. Xu and Y. Gao, Conjugated Microporous Polymers Based on Octet and Tetratopic Linkers for Efficient Iodine Capture, *ACS Appl. Mater. Interfaces*, 2023, **15**, 46408-46416.
20. Z.J. Li, Z. Yue, Y. Ju, X. Wu, Y. Ren, S. Wang, Y. Li, Z.-H. Zhang, X. Guo, J. Lin and J.-Q. Wang, Ultrastable Thorium Metal–Organic Frameworks for Efficient Iodine Adsorption, *Inorg. Chem.*, 2020, **59**, 4435-4442.

21. P. Chen, X. He, M. Pang, X. Dong, S. Zhao and W. Zhang, Iodine Capture Using Zr-Based Metal–Organic Frameworks (Zr-MOFs): Adsorption Performance and Mechanism, *ACS Appl. Mater. Interfaces*, 2020, **12**, 20429-20439.
22. Z. Zhang, Y. Chen, Y. Sun, Z. Chen, Z.-Y. Zhang, F. Liang, D. Liu and H.-C. Hu, Post-synthetic modification of zeolitic imidazolate framework-90 via Schiff base reaction for ultrahigh iodine capture, *J. Mater. Chem. A*, 2023, **11**, 23922-23931.
23. R.X. Yao, X. Cui, X.-X. Jia, F.-Q. Zhang and X.-M. Zhang, A Luminescent Zinc(II) Metal–Organic Framework (MOF) with Conjugated π -Electron Ligand for High Iodine Capture and Nitro-Explosive Detection, *Inorg. Chem.*, 2016, **55**, 9270-9275.
24. X.H. Xu, Y.X. Li, L. Zhou, N. Liu and Z.-Q. Wu, Precise fabrication of porous polymer frameworks using rigid polyisocyanides as building blocks: from structural regulation to efficient iodine capture, *Chem. Sci.*, 2022, **13**, 1111-1118.
25. L. Xu, Q. Zheng, Y. Wang, L. Jiang, J. Jiang and J. Qiu, A pillared double-wall metal-organic framework adsorption membrane for the efficient removal of iodine from solution, *Sep. Purif. Technol.*, 2021, **274**, 118436.
26. Y. Xie, T. Pan, Q. Lei, C. Chen, X. Dong, Y. Yuan, W. A. Maksoud, L. Zhao, L. Cavallo, I. Pinnau and Y. Han, Efficient and simultaneous capture of iodine and methyl iodide achieved by a covalent organic framework, *Nat. Commun.*, 2022, **13**, 2878.
27. Z. Zheng, Q. Lin, Y. Gao, X. Ji, J. L. Sessler and H. Wang, Recent advances in iodine adsorption from water, *Coord. Chem. Rev.*, 2024, **511**, 215860.
28. R. Liu, W. Zhang, Y. T. Chen, C. Xu, G. Z. Hu and Z. Han, Highly efficient adsorption of iodine under ultrahigh pressure from aqueous solution, *Sep Purif Technol*, 2020, **233**, 115999.
29. Y. S. A. Ghanem, F. Vakil, K. M. A. Qasem, M. A. S. Salem, M. Z. A. Warshagha, Z. Nusrat and M. Shahid, An yttrium-organic framework for effective iodine capture and sensing of Cr^{6+} ions, *Inorg. Chem. Commun.*, 2024, **159**, 111800.
30. M. El-Shahat, A. E. Abdelhamid and R. M. Abdelhameed, Capture of iodide from wastewater by effective adsorptive membrane synthesized from MIL-125-NH₂ and cross-linked chitosan, *Carbohydr. Polym.*, 2020, **231**, 115742.
31. W. Zhou, A. Li, M. Zhou, Y. Xu, Y. Zhang and Q. He, Nonporous amorphous superadsorbents for highly effective and selective adsorption of iodine in water, *Nat. Commun.*, 2023, **14**, 5388.

32. S. Maji and R. Natarajan, A halogen-bonded organic framework (XOF) emissive cocrystal for acid vapor and explosive sensing, and iodine capture, *Small*, 2023, **19**, 2302902.
33. W. Xie, D. Cui, S. Zhang, Y. Xu and D. Jiang, Iodine capture in porous organic polymers and metal-organic frameworks materials, *Mater. Horiz*, 2019, **6**, 1571-1595.
34. M. Huang, L. Yang, X. Li and G. Chang, An indole-derived porous organic polymer for the efficient visual colorimetric capture of iodine in aqueous media via the synergistic effects of cation- π and electrostatic forces, *Chem. Commun.*, 2020, **56**, 1401-1404.
35. X.-J. Zhao, S. Liu and J. Sun, Hierarchically Porous Poly(ionic liquid) – Organic Cage Composite Membrane for Efficient Iodine Capture, *Chem. Eur. J*, 2022, **28**, e202201199.
36. R. Zia Mah, J. Park, Y. Kim Jung, I. Kim Kwang and S. Mushtaq, A Review of Nanoparticles Utilized in the Removal of Radioactive Iodine from Wastewater Streams, *J. radiopharm. mol. probes*, 2024, **10**, 43-49.
37. W. X. Wu, H. C. Liu and W. J. Jin, Halogen Bonding Adsorbent Pyridine N-oxides for Iodine Capture in Water, *Chem. Eur. J*, 2022, **28**, e202103336.